We are IntechOpen, the world's leading publisher of Open Access books Built by scientists, for scientists

4,800
Open access books available

122,000
International authors and editors

135M
Downloads

Our authors are among the

154
Countries delivered to

TOP 1%
most cited scientists

12.2%
Contributors from top 500 universities

WEB OF SCIENCE™

Selection of our books indexed in the Book Citation Index in Web of Science™ Core Collection (BKCI)

Interested in publishing with us?
Contact book.department@intechopen.com

Numbers displayed above are based on latest data collected.
For more information visit www.intechopen.com

26

GCMC Simulations of Gas Adsorption in Carbon Pore Structures

Maria Konstantakou, Anastasios Gotzias,
Michael Kainourgiakis, Athanasios K. Stubos and Theodore A. Steriotis
National Center for Scientific Research Demokritos
15310 Ag. Paraskevi, Athens,
Greece

1. Introduction

The development of algorithms about 50 years ago gave to the scientific community an extremely powerful tool, allowing the utilization of digital computers to simulate and predict the thermodynamic, structural and dynamic properties of bulk fluids. The most widely used simulation methods for molecular systems are Monte Carlo and Molecular Dynamics. These methods provide a link between microscopic (molecular level) and macroscopic behavior, by simply evaluating numerically fundamental equations of statistical mechanics. Their great advantage is the ability to treat large systems having big number of molecules in relatively small time.

In the beginning, due to the limited computer power and availability, the studies were focused on the investigation of properties of the simplest possible fluid model (hard sphere) in the bulk state in two and three dimensional systems. The very first computer simulation of a liquid was carried out at the Los Alamos National Laboratory by Metropolis in 1953 (Metropolis et al., 1953). The technique employed, i.e. "Metropolis Monte Carlo", uses a Markov chain to generate a series of molecular configurations (microstates) by stepping from one configuration to the next with appropriate probability rules (Allen & Tildesley, 1987; Frenkel & Smit, 1996). Finally, the requested quantities (thermodynamic properties of interest) can be averaged over the configurations.

The rapid increase of computer resources promoted the scientific interest to explore the behavior of more complex systems, such as the thermodynamic properties of gas molecules confined in small cavities. In this case, beyond the calculation of the interactions between a molecule and the surrounding fluid, the solid adsorbent must be accurately reproduced and adsorbate–adsorbent interactions must also be considered. The first theoretical studies aiming to investigate the phenomenon of gas adsorption in porous solids were published in the 1960's (Alder & Wainwright, 1960). Since then, a large number of theoretical studies has been published, comparing experimental and simulation results and thus evaluating the accuracy of the models (gas–solid and gas-gas interactions) employed. Nowadays, computer simulation of gas adsorption is considered to be an extremely useful tool for explaining and analyzing experimental results but also for predicting gas solid equilibria.

Adsorption in porous materials is utilized in several industrial (food, pharmaceutical and petrochemical industry) and geophysical applications, for pollution control and

environmental protection, mixture separation, water purification and gas storage (Ruthven, 1984). Moreover, gas adsorption measurements are widely used in materials science as a reliable method for the characterization of porous materials (Gregg & Sing, 1982; Lowell & Shields, 1991). The better understanding of the detailed mechanism that takes place during these operations is essential for designing improved processes. The materials that are commonly used in these fields are crystalline, ordered, and amorphous porous materials, such as zeolites, amorphous silica and alumina, activated carbons, metal-organic frameworks (MOFs) and other advanced materials. The large surface areas of these materials and the confinement offered by their extended pore network enhance their catalytic, sorptive and separation activity.

Porous materials are classified by the International Union of Pure and Applied Chemistry (IUPAC) in micropores with pore diameters less than 2 nm, mesopores having pore widths between 2 and 50 nm and macropores with pore diameters greater than 50 nm (Everett, 1972). The pore width is defined as the diameter (D) in the case of cylindrical pores or as the distance between opposite walls (H) in the case of slit-shaped pores. Modern industrial and technological needs has led materials science (and vice versa) towards the development of novel materials having extremely small pore widths. The size of these pores is approaching few molecular diameters and materials with such pore systems reveal a wide range of properties, that differ significantly from mesopores and big micropores. Adsorption depends strongly on the structural properties of the adsorbent material, e.g. the specific surface area, the porosity and the pore dimensions. In general, the existence of a large specific surface area and of an extensive number of readily accessible small sized pores is desirable as in pores of molecular dimensions the adsorbent field is further intensified due to the overlapping solid wall potentials, resulting in enhanced adsorption capacity.

The pore filling mechanism is sufficiently described for the case of mesopores and macropores. The Kelvin equation is a purely thermodynamic model that applies at subcritical temperatures and relates the relative pressure (P/P_0) at which capillary condensation occurs to the pore width (Gregg & Sing, 1982). However, the equation fails to apply in micropores, mainly because, a "real" adsorbate phase of molecular dimensions cannot be defined. Molecular models, as for instance the Density Functional Theory (DFT) (Seaton et al., 1989; Lastoskie et al., 1993; Aukett et al., 1992; Ravikovitch et al., 1995; Sosin & Quinn 1995; Scaife et al., 2000; Jagiello & Thommes 2004; Nguyen & Bhatia 2004) and the Monte Carlo (MC) technique (Nilson et al., 2003; Do & Do 2005; Nguyen et al., 2005), can offer a more comprehensive representation of the pore filling process. DFT is computationally less demanding and can provide an accurate description when dealing with simple fluids (spherical molecules) and simple geometries. However, as the precision of the microscopic models depends principally on the truthful representation of the molecules, including partial charges and atom sites, MC has been established as an efficient alternative approach. The method can give valuable information concerning the densification process in nanopores and moreover details about the packing structure of the gas molecules inside the pore can be extracted from the local density and molecule orientation profiles (Samios et al., 1997; Samios et al., 2000).

The MC method is widely applicable in carbon materials with large number of studies referring to the adsorption of different gases like hydrogen, carbon dioxide, methane, nitrogen, argon etc., for several applications. For example, during the last decade, the scientific community exhibited considerable interest about physical adsorption of hydrogen on various carbon based nanoporous materials. Likewise, adsorption in porous solids might

provide a useful tool for handling the challenging environmental issue of the high CO_2 atmospheric concentrations. The activities undertaken involve CO_2 separation, collection and finally storage in geologic formations (such as oil and gas fields, coal beds and saline formations). Thus, the knowledge of the behavior of CO_2 molecules during sorption in confined spaces like nanopores is of paramount importance. On the other hand, gas adsorption is used widely for the characterization of porous carbons, in terms of pore size distribution (PSD). The method combines experimental and simulated adsorption isotherms of gases like N_2, CO_2, Ar and lately H_2 (or combinations of them), in order to calculate the optimal distribution of the pore sizes of a material.
In this work the Grand Canonical Monte Carlo (GCMC) method is employed for the study of the adsorption behavior of H_2, CO_2 and N_2 in three different carbon structures (slits, tubes and cones). Initially, the construction of solids, the representation of the gas molecules and the modeling of all the types of interactions are described. The significance of choosing the right potentials is emphasized, by giving an example about the H_2 quantum contribution at low temperatures. The influence of the pore size and geometry, as well as the temperature dependence is examined while the GCMC method is also used to study the packing structure of the gas molecules in the pores (local density and orientation profiles) as the temperature or pressure change. Finally, the simulated results are employed for the determination of pore size distribution of carbon porous materials.

2. Simulation model

Depending on the thermodynamic equilibrium properties sought a variety of Monte Carlo ensembles is available (Allen & Tildesley, 1987). The GCMC method describes a collection of microscopic systems of equal volumes in contact with a heat bath and a particle reservoir, i.e. the systems have fixed volume (V), temperature (T) and chemical potential (μ) (Nicholson & Parsonage, 1982). Each microscopic system (microstate) is literally an identical simulation box containing a reliable representation of the pore under investigation and a unique configuration of adsorbate particles determined by the applied μ and T. As under these conditions GCMC permits fluctuations in density and energy the microstates are heuristically sampled and the averages of the fluctuating quantities are evaluated. The adsorption isotherm is then expressed as the output density (or the average number of adsorbate molecules) versus chemical potential ($N=f(\mu)$) at a fixed temperature. The generation of different microstates is based on a Markov chain process, i.e.. from any given molecular configuration a new one is generated by random insertion, deletion or displacement of an adsorbate molecule. If molecules are not spherical all moves are accompanied by random rotation (Marsaglia algorithm, Allen & Tildesley, 1987). Microstates are accepted with a probability that depends on the energy difference between the new (trial) and the old (current) configuration. According to the Metropolis sampling scheme random displacement is accepted with a probability $p_{move} = \min\left[\exp(-\Delta U / kT);1\right]$: The acceptance probability of insertion is :

$$p_{ins} = \min\left[\frac{V}{N+1}\exp(\frac{\mu-\Delta U}{kT});1\right] \quad (1)$$

while for the particle deletion :

$$p_{del} = \min\left[\frac{N}{V}\exp(\frac{\Delta U - \mu}{kT});1\right] \quad (2)$$

where $\Delta U = U_{new} - U_{old}$ is the potential energy change between the new (trial) and old (current) configuration. The acceptance probability of any new configuration is independent of configurations older than the current. A detailed presentation of the method is described elsewhere (Nicholson & Parsonage, 1982; Allen & Tildesley, 1987). The presence of the adsorbing surface requires the application of periodic boundary conditions depending on the pore geometry. For slit and cylindrical models boundary conditions are applied in the directions other than the width and the diameter respectively, while in the case of the carbon cones periodic conditions are applied in all directions. In our case, each simulation box contains an isolated pore model (slit, cylinder or cone) and statistics are studied only inside the structures (external surface is omitted). In the case of periodic structures (slits and tubes), the size of the box can be varied in order to ensure that at least 500 particles remain in the simulation box at each pressure. The simulations run typically for $7x10^6$ configurations, while statistics are not collected over the first $3x10^6$ configurations to assure adequate convergence of the simulation.

2.1 Simulation models

2.1.1 Gas molecules representation - adsorbate - adsorbate interactions

(a) Hydrogen molecule

In general the interaction potential of two particles (i and j) is given by Lennard-Jones (LJ):

$$u_{ij} = 4\varepsilon_{ij}\left[\left(\frac{\sigma_{ij}}{r_{ij}}\right)^{12} - \left(\frac{\sigma_{ij}}{r_{ij}}\right)^{6}\right] \quad (3)$$

where ε_{ij} and σ_{ij} are the characteristic energy and collision diameter of those particles and r_{ij} is the distance between them. Hydrogen can be treated either as one center (spherical) or as a two center (linear) particle. The parameters for the spherical representation are ε_{HH}/k_B = 36.7 K and σ_{HH} = 0.2958 nm (Darkrim & Levesque, 1998) and for the two-site model are ε_{HH}/k_B = 12.5 K and σ_{HH} = 0.259 nm, while the H–H distance is assumed to be the actual bond length (0.074 nm) (Cracknell, 2001). Apart from classic (LJ) interaction, H_2 reveals also a quantum behaviour that can contribute significantly to adsorption especially under confinement and/or low temperatures (Sese, 1995; Wang & Johnson, 1999; Tanaka at al., 2005). Thus a correction term is added to the LJ potential and interactions are calculated by the so called Feynmann and Hibbs quantum corrected expression :

$$u_{ij}\big|_{FH} = u_{ij} + \left(\frac{\beta\hbar^2}{24\mu_m}\right)\nabla^2\left(u_{ij}\right) \quad (4)$$

where $\beta=(k_bT)^{-1}$, $\hbar=h/2\pi$ (h is the Plank constant), μ_m is the reduced mass of a pair of interacting molecules ($\mu_m=m/2$) and u_{ij} is the energy of the pairwise LJ interaction.

(b) Carbon dioxide molecule

CO_2 is modeled as a three charged center LJ molecule with ε_{OO}/k_B = 80.507 K, σ_{OO} = 0.3033 nm, ε_{CC}/k_B = 28.129 K, σ_{CC} = 0.2757 nm (Harris & Yung, 1995). The O-O and C-O distances are 0.2298 nm and 0.1149 nm respectively. The model was obtained after suitable optimization

of literature LJ parameters (Murthy et al., 1983), and has the advantage of predicting fairly well the phase coexistence curve and the critical properties of the fluid.
The intermolecular potential $u_{CO_2-CO_2}$ is assumed to be a sum of the interatomic potentials between the atoms of the interacting molecules, plus the electrostatic interactions due to CO_2 quadrupole moment with point partial charges $q_1 = q_3 = -0.3256e$ and $q_2 = +0.6512e$ (Eq.5):

$$u\big|_{CO_2-CO_2} = \sum_{i=1}^{3}\sum_{j=1}^{3}\left(u_{ij} + \frac{q_i q_j}{4\pi\varepsilon_o r_{ij}} \right) \tag{5}$$

where ε_0 is the permittivity of vacuum. The indices i (j) refer to the sites of the first (second) interacting molecules. All cross interaction potential parameters between two sites, are calculated according to the Lorentz-Berthelot rules ($\sigma_{ij}=(\sigma_{ii}+\sigma_{jj})/2$, $\varepsilon_{ij}=(\varepsilon_{ii}\varepsilon_{jj})^{1/2}$).

(c) Nitrogen molecule

N_2 is modelled as a two center LJ molecule (Kuchta & Etters, 1987).The parameters used are ε_{NN}/k_B = 37.8 K and σ_{NN} = 0.3318 nm, with the two centers separated by 0.1094 nm. The molecule has a quadrupole moment with the four point charges $q_1 = q_4 = +0.373e$ and $q_2 = q_3 = -0.373e$ placed along the molecular axis at positions 0.0847 nm and 0.1044 nm from the center respectively. The intermolecular interactions were calculated according to:

$$u\big|_{N_2-N_2} = \sum_{j=1}^{2}\sum_{i=1}^{2} u_{ij} + \sum_{k=1}^{4}\sum_{l=1}^{4}\frac{q_k q_l}{4\pi\varepsilon_o r_{kl}} \tag{6}$$

where i and k or j and l refer to the LJ and charge centers of the first or second interacting molecules.

2.1.2 Carbon structures – adsorbate / adsorbent interactions

(a) Slit–shaped pores

Due to the layered graphitic structure, the majority of porous carbons possess slit like pores. Graphitic surfaces can be simulated by stacked planes of LJ carbon atoms separated by Δ=0.335nm and having a number density ρ_w=114 atoms/nm^3 (figure1). Assuming the classic Lennard – Jones potential for the fluid – wall atom interactions and integrating over all atoms of all graphite planes, the '10-4-3' potential of Steele is deduced (Steele, 1974):

$$u_w(r_z) = 2\pi\rho_w\varepsilon_{\alpha\beta}\sigma_{\alpha\beta}^2\Delta\left[\frac{2}{5}\left(\frac{\sigma_{\alpha\beta}}{r_z}\right)^{10} - \left(\frac{\sigma_{\alpha\beta}}{r_z}\right)^{4} - \frac{\sigma_{\alpha\beta}^4}{3\Delta(0,61\Delta + r_z)^3}\right] \tag{7}$$

where r_z is the distance between a Lennard – Jones site of an adsorbate molecule and the solid surface. The potential parameters of the solid surface are ε_{ss}/k_B =28.0 K and σ_{ss}=0.34 nm, while all the cross interaction potential parameters between different sites are calculated according to the Lorentz-Berthelot rules. The same ε_{ss} and σ_{ss} parameters are used for the cylindrical and the conical carbon structures.
The overall potential energy U_w due to the walls inside a slit-like pore is calculated by the sum of the interactions between the adsorbate and both pore walls:

$$U_w = u_w(r_z) + u_w(H - r_z) \tag{8}$$

where H is the distance between the pore walls (physical width).
For interacting with hydrogen slits the F-H quadratic term has to be added to the above expression. In this case this term is (Tanaka et al., 2005):

$$u_{qu}(r_z) = 176\pi\rho_s\varepsilon_{\alpha\beta}\frac{\beta\hbar^2}{24\mu_m}\sum_{j=0}^{2}\left[\frac{1}{2}\left(\frac{\sigma_{\alpha\beta}}{r_z+j\Delta}\right)^{12} - \frac{1}{4.4}\left(\frac{\sigma_{\alpha\beta}}{r_z+j\Delta}\right)^{6}\right] \quad (9)$$

so that the total solid-fluid potential, $u_{H\text{-}w}$, is given by:

$$u_{H-w}(r_z) = u_{10-4-3}(r_z) + u_{qu}(r_z) \quad (10)$$

where r_z is the distance between the LJ site on the adsorbent and the plane of carbon atoms, μ_m is the reduced mass and ρ_s=38.19 nm^{-2} the surface density of a single graphite layer.

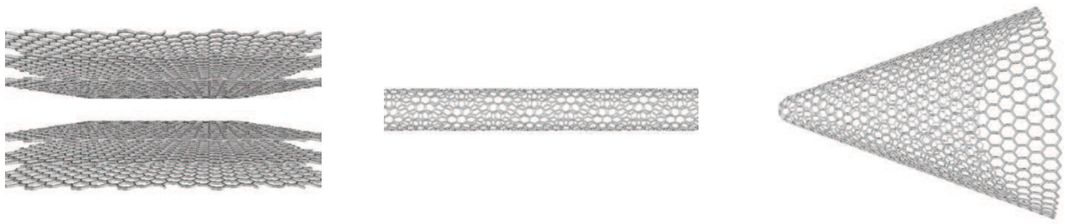

(a) (b) (c)

Fig. 1. The carbon pore models a) slit-shaped, b) nanotube and c) cone

(b) Carbon nanotubes

Carbon nanotubes (CNTs) production was first reported by Iijima (Iijima, 1991). A single wall carbon nanotube (SWNT) is generated (Dresselhauss et al., 1996) by rolling up a graphene sheet into a seamless cylinder (Figure 1). CNT structures are represented by the chiral vector, i.e. a pair of indices (n,m) referred where n and m are scalars on the principal unit vectors of the graphene lattice. The diameter of the nanotube is then given by : $d = \frac{a}{\pi}\sqrt{(n^2+nm+m^2)}$ where a = 0.246 nm. The fluid-solid interactions are calculated from equation 4, where the reduced mass of a carbon and a hydrogen atom is: $\mu_m = 7/12$.

(c) Carbon cones

Carbon cones (CCs) are one of the newest carbon structures, revealing unique electronic, chemical and mechanical properties (Heiberg-Andersen & Skjeltorp, 2007; Heiberg-Andersen et al., 2008). CCs were first observed in 1994 (Ge & Sattler, 1994), while bulk quantities of conic structures with five different apex angles were produced later in an industrial process (Krishnan et al., 1997). CC models are also produced by cutting out of a graphene sheet one up to five 60° sectors of and joining the dangling bonds. This procedure introduces 1 up to 5 pentagons in the graphene structure. Therefore, the possible apex angle φ can obtain the discrete values of 112.9°, 83.6°, 60.0°, 38.9° and 19.2° (in accordance with the 5 different observed "real" structures) given by the equation $\sin(\varphi/2) = (2\pi - p\pi/3)$ for p = 1, 2, ..., 5, respectively (p is the number of pentagons). Each of the five cone structures used in this work contains approximately 2000 carbon atoms and is terminated by hydrogen atoms. The solid-fluid interaction potentials are computed again by equation 4.

3. Results and discussion

3.1 The pore wall influence

When a molecule is confined within a pore it interacts with the whole structure resulting in a "complex" potential energy field that depends on the pore shape and width. In narrow micropores (<1nm), the gas-solid interactions are extremely strong, due to the overlapping potentials of opposing walls (Figure 2) and a single energy minimum located at the center of the pore exists. For even smaller pore sizes the repulsive contributions of the opposite walls start to interfere, leading to reduced attraction (i.e. reduced potential well depth). As pore size increases, the solid - fluid potential has two shallow minima and interactions at the center of the pore tend to become negligible. A comparison of the potential functions between slit – shaped and cylindrical pore models of the same dimension (similar pore widths) shows that the curvature of the surface results in deeper minima, i.e. stronger interactions for carbon nanotubes than for slit-shaped pores (Figure 2).

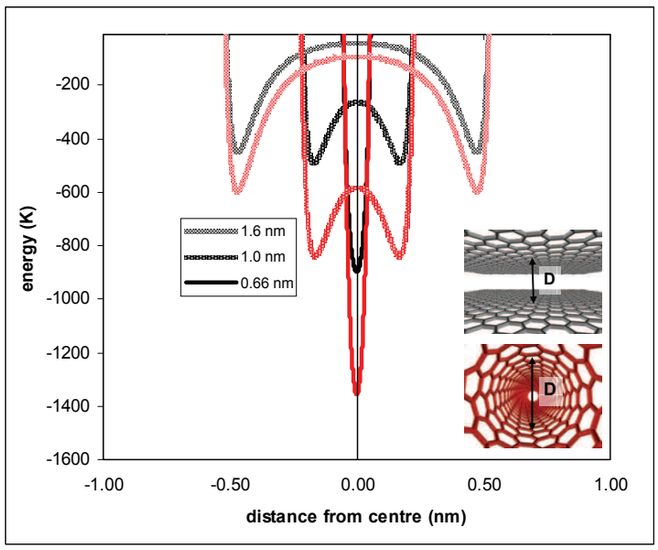

Fig. 2. Hydrogen interaction potential profiles inside carbon slit and nanotube models for three different widths or diameters respectively. Interaction curves are plotted against the distance from the centre.

The interaction potential of a gas molecule inside CCs is similar, however it depends strongly on the distance from the tip since the effective pore width increases linearly with it. Examples of the potential profiles inside CC cavities are presented in figure 3 for regions of high confinement (close to the tip) where interactions are enhanced and obtain a single minimum (a), but also far from the tip (b) (where the diameter is 1nm (Gotzias et al., 2010)).

(a) Quantum effects

The contribution of quantum effects on adsorption phenomena depends on the temperature and the density of the fluid inside nanopores. Generally, the quantum behaviour is equivalent to an enlargement of the effective molecule diameter and thus leads to a decrease of the amount adsorbed. A simple criterion regarding the validity of treating a quantum – mechanical system using the classical approach, is based on the de Broglie thermal wavelength Λ calculation (Hansen & McDonald, 1990), given by:

$$\Lambda = \frac{h}{\sqrt{2\pi m k_B T}} \tag{11}$$

where h is the Planck's constant m is the mass of an atom, T is the temperature and k_B is the Boltzmann's constant. Classical approximations are justified, when the ratio Λ/a is much less than unity ($a \cong \rho^{-1/3}$, where ρ is the fluid density). For example, for Ar the ratio is around 0.1 at the triple point (T=83.8K). Hydrogen is much lighter, Λ/a = 0,94 at its triple point (T=13.8K) and thus the quantum effects cannot be neglected. Furthermore, Λ/a changes when hydrogen molecules are confined in the narrow micropores, where the strong adsorption potential leads to fluid densification (Liu et al., 1999).

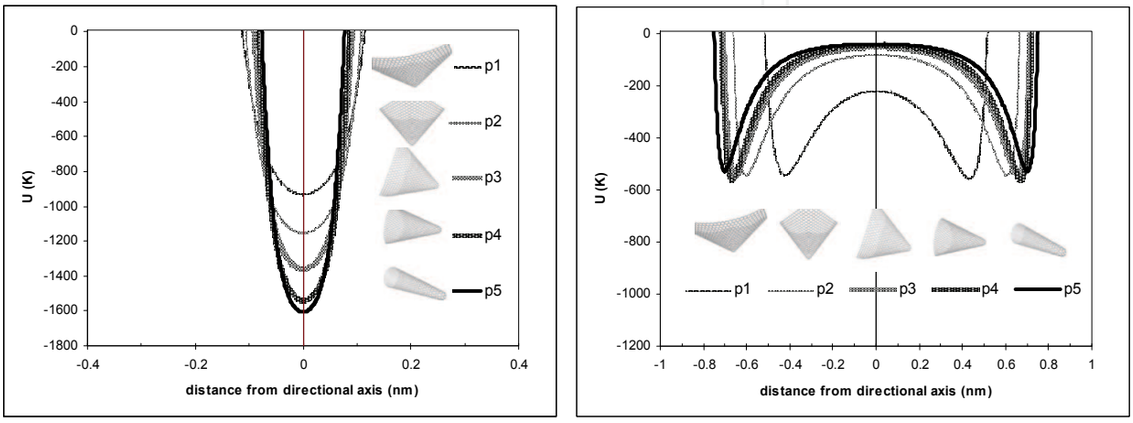

(a) (b)

Fig. 3. Interaction profiles inside the five conic cavities. The curves correspond to interaction profiles along the radial distance normal to the cone directional axis a) close to the tip and b) at a circular cone-plane intersection of 1nm diameter

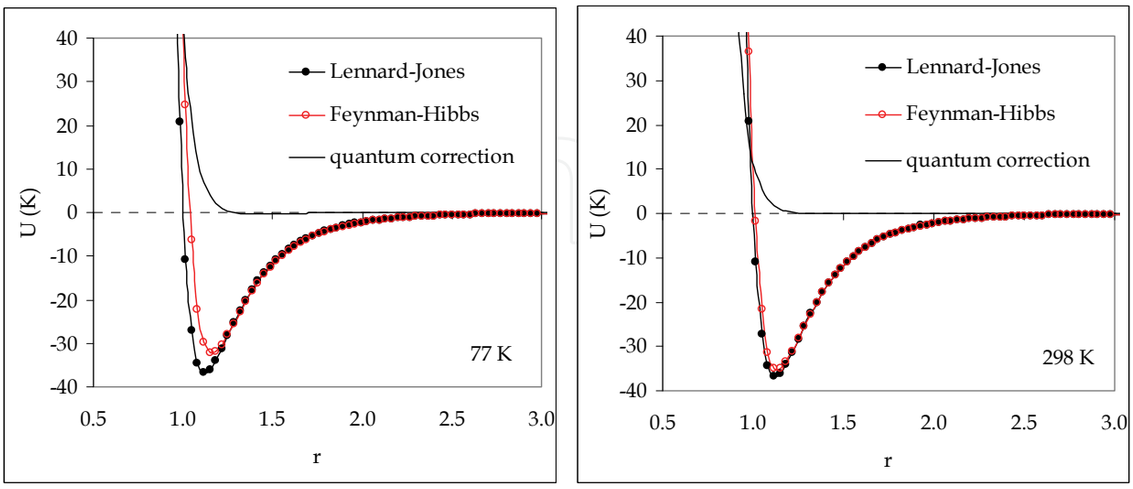

(a) (b)

Fig. 4. Classical and Feynman – Hibbs corrected fluid-fluid interaction potential at 77 and 298 K. For comparison the quantum correction has been also plotted.

The results of applying the Feynman – Hibbs effective potential in the fluid - fluid and solid – fluid interactions are demonstrated in figures 4 and 5 at 77 and 298K. Figure 4 presents the total quantum corrected fluid – fluid interaction potential, as well as the classical LJ potential and the quantum contribution calculated by the Feynman – Hibbs method. At low temperature (figure 4a), the quantum contribution is evident, since the total potential reveals weaker interaction between the fluid molecules, than the classical one. On the other hand, at room temperature (figure 4b) the two potentials are very close to each other, however, the classical potential still overestimates slightly the interaction energy.
The differences are more clear when examining the solid – fluid interactions, especially in very small pores. Figure 5 presents the classical and the total quantum corrected solid – fluid interaction potential for selected slit pores. Similarly to the case of fluid – fluid interactions, the classical LJ potential overestimates the interaction energy, while the effect of quantum behaviour depends strongly on the pore size, varying from strong (in smallest pores) to negligible (wide pores).

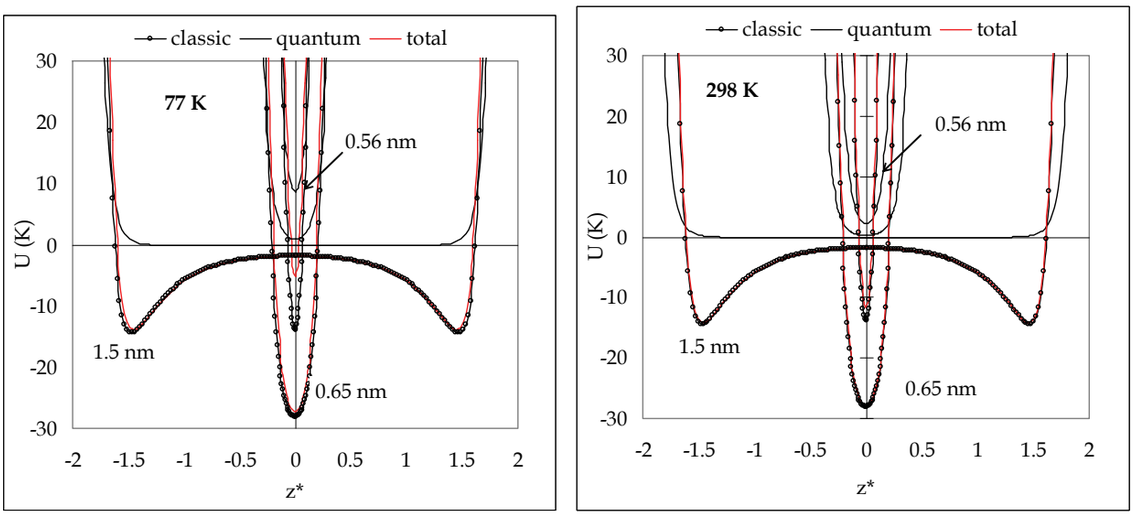

(a) (b)

Fig. 5. Classical and Feynman – Hibbs corrected solid-fluid interaction potential at a) 77 and b) 298 K for different slit sizes (the quantum term is also presented). z* is the reduced distance from the center ($z^*=z/\sigma_{HH}$).

3.2 GCMC simulation results – adsorption isotherms

(a) Hydrogen adsorption

GCMC simulations have been carried out for the calculation of the adsorption isotherms of hydrogen in the three carbon structures described above, for pore sizes ranging from about 0.6 to 2.0 nm. The calculations have been performed for discrete pore sizes (per ~0.1nm pore width) for slit-shaped and cylindrical pores (H or D up to 2.0nm respectively) and for the five possible carbon cones (1-5 pentagons). For comparison, in the cones case, statistics were collected in conic segments of equal volume (30nm^3). The simulated isotherms at 77 K and pressures up to 20 bar are presented in figures 6a, 6b (slits and nanotubes respectively) and 7 (cones). For comparison a set of simulated adsorption isotherms at 298K is also presented.

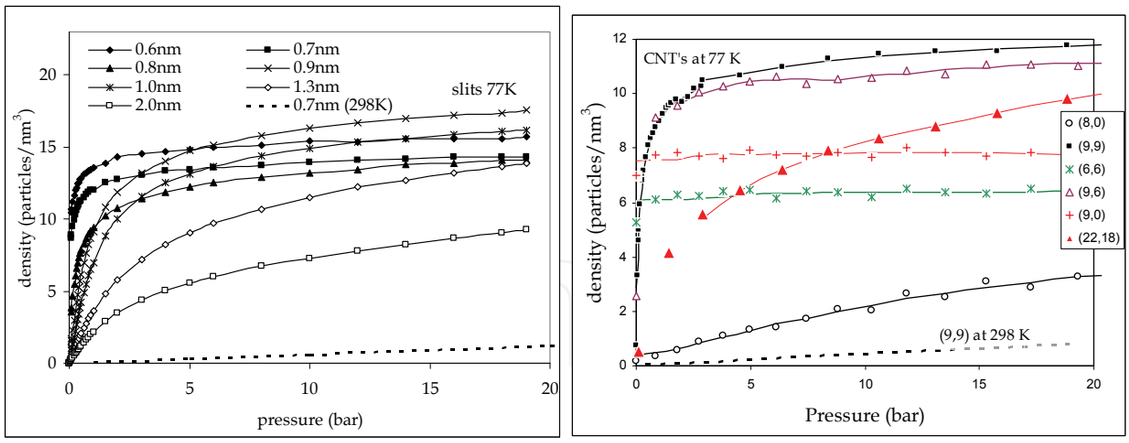

(a) (b)

Fig. 6. Calculated adsorption isotherms for hydrogen at 77K in a) slit-shaped pores and b) nanotubes

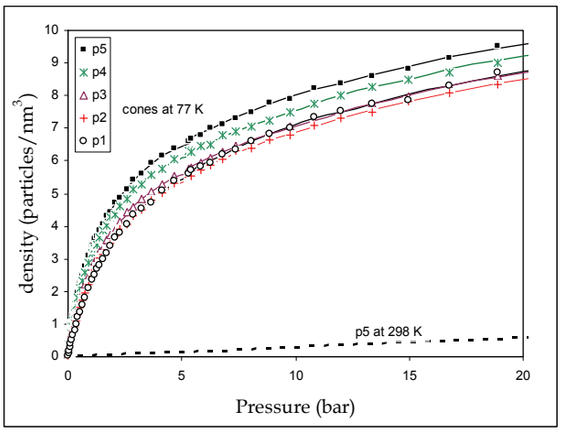

Fig. 7. Hydrogen adsorption densities at 77K corresponding to the five conic cavities of 30 nm^3 volume. The isotherm at 298K for the p5 is also shown.

In the pressure range studied at narrow pores (pore width < 1.0 nm for the slit – shaped and cylinders), the isotherms are of Langmuir type (according to IUPAC classification). Adsorption is particularly enhanced at low pressures, due to the overlapping solid-fluid interaction potential. The very small pores (<0.9nm) are completely filled with hydrogen even for relatively low pressures (≈ 1 bar), and no increase of the amount adsorbed is observed at higher pressures, due to pore volume limitations. As the pore sizes increase the wall interactions grow weaker affecting merely the molecules close to the pore walls, and adsorption is mainly determined by the available pore volume. Therefore isotherms tend to become of Henry type (i.e. straight lines). Similar conclusions are deduced from figure 6b, regarding carbon nanotubes. The basic difference compared to the slit-shaped pores is the much lower density values observed in the fine pores. This can be attributed to the loss of one degree of freedom of the molecules when confined in cylinders, i.e. the system is actually 2D in slits and 1D in cylinders. The nanotubes illustrated in Figure 6b have comparable pore size (diameter) to the slits of figure 6a ((8,0) ~ 0.62nm, (9,0) ~ 0.7nm, (6,6) ~ 0.8nm, (9,6) ~ 1.02nm, (9,9) ~ 1.22nm and (22,18) ~ 2.7nm).

In carbon cones, the differences are less emphasized compared to the slit and cylindrical geometries. The cone heterogeneity, resulting mainly from the curvature gradient along the surface, affects the adsorption process at low pressures where adsorption on the very high energy sites (close to the tip) occurs. After filling these sites the cones reveal a constantly increasing isotherm curve. At low pressures the more "narrow" cones (more pentagons on the tip) have increased adsorption capacity due to stronger confinement, in accordance with the interaction potential profiles of Figure 3. It is however interesting to note that for pressures above 4 bar the capacity of p1 is slightly higher than those of p2 or even p3. This should be expected since at this pressure range adsorption occurs at the core of the pore. There the interaction in p1 is stronger since it has a lower local energetic minimum (Fig. 3b) as the distance from the tip (height) is shorter than the other cones.

(b) Carbon dioxide adsorption

Carbon dioxide adsorption in nanopores shows many differences from hydrogen. The main reason for this is that while H_2 is supercritical at 77K the critical temperature of carbon dioxide is 31.25°C (304.4K), i.e. high enough to be liquefied even at room temperature. The shape of the isotherms changes gradually, revealing capillary condensation at pressures far below the vapour pressure. The condensation pressure and consequently the final form of the adsorption isotherm, is determined by the pore size and geometry, and also by the fluid-fluid and fluid-solid interaction. In this respect, the carbon dioxide adsorption isotherms in slit-shaped and cylindrical pore models were calculated using the GCMC method at a) 195.5 K the dry ice temperature, below the triple point b) 253 K, where the full (0 – 1) relative pressure range is attained with experimental sorption tests at modest pressures (e.g. up to 20 bar), c) 273 K, a temperature where many adsorption experiments are typically carried out, d) 298 K (room temperature) and e) 308 K, slight above the critical temperature.

The carbon dioxide isotherms obtained by the GCMC simulations for typical slit – shaped pores of selected sizes (*H* up to 2.0 nm) and temperatures are presented in Fig. 8. Detailed pertinent work is reported elsewhere (195.5 and 308K: Samios et al., 1997 ; Samios et al., 2000, 253 and 298 K Konstantakou et al., 2007a, Konstantakou et al., 2007b, 195.5, 253 and 273 K Konstantakou et al., 2010). As expected, higher adsorption capacities are observed as temperature decreases. The adsorption mechanism can be divided into three regions: initially at small pressures, micropore filling occurs, where the gas molecules occupy the whole pore space adjacent to the walls, and adsorption is almost entirely controlled by the solid - fluid interactions; at higher pressures, the interaction is getting relatively weaker resulting to a reduced isotherm slope and multiple adsorbed layers are developed in larger pores. The capillary condensation phenomenon takes place abruptly with an almost vertical transition from the gas-like to the liquid-like phase, and the condensation pressure is unique for each pore size, geometry and temperature applied. For this reason such CO_2 computed isotherms can be used for deducing the pore size distribution of porous solids.

Depending on the pore size and the temperature the isotherm may not display all three regions. For example, in very narrow pores (e.g. 0.8 nm) instead of multilayer adsorption/capillary condensation, due to confinement the prevailing mechanism is micropore filling giving rise to Langmuir type isotherms. As the pore size increases (e.g. 1.2 nm) more pore space is available but the wall attraction is weaker and pore filling occurs at higher pressures. For larger pores the isotherm is transformed to type IV. The observed sudden uptake corresponds to the capillary condensation transition. The pores are filled with the liquid – like phase and no further increase in adsorption is observed with pressure.

For wide enough pores, where the wall attraction is almost negligible the fluid density value is approaching the bulk one. Considering the cylindrical geometry, carbon dioxide behavior appears to be rather similar to the slits, except from the smoother densification process. In addition, much lower density values are calculated for the very narrow pores (0.65 nm) contrary to the slits (0.6 nm). For a cylindrical pore, reduction in pore diameter will lead to one-dimensional behavior. As a consequence, molecules cannot attain the most energetically favorable orientation inside the pore and thus pack efficiently, as they are forced to align in a way almost parallel to the pore axis.

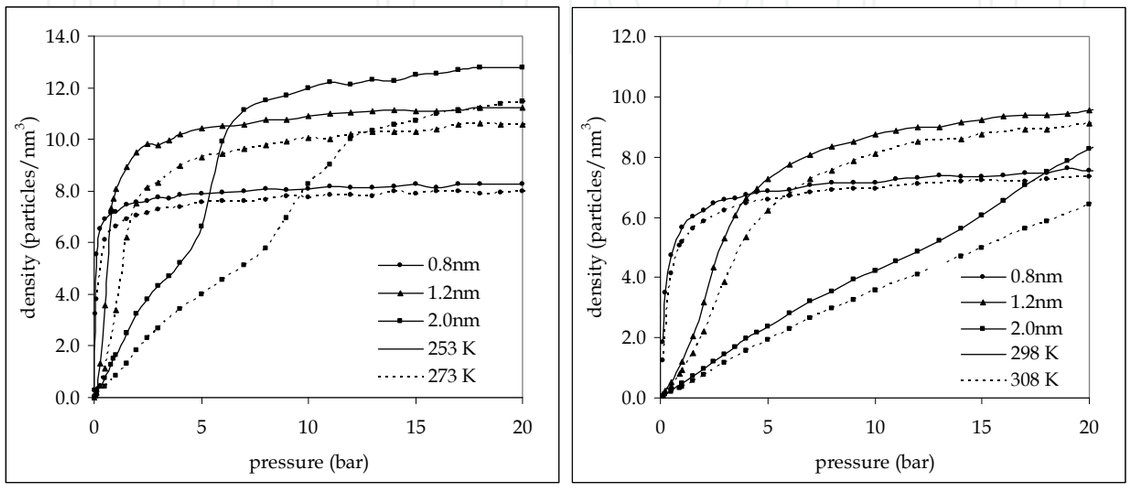

Fig. 8. Carbon dioxide adsorption densities for selected slit pores and temperatures.

In general, the gas-liquid phase transition in pores (capillary condensation) is a very interesting feature, which is observed when condensable gases are confined in small cavities. The phenomenon has been extensively studied in pores of various geometries both experimentally and theoretically (Evans & Tarazona, 1984 ; Ravikovitch et al., 2001 ; Nilson & Griffiths, 1999 ; Neimark et al., 2003). Capillary condensation takes place at pressures below the bulk condensation pressure at a given temperature. The relative pressure where pore condensation appears depends on the liquid interfacial tension, the strength of the attractive interactions among the fluid and pore walls, the pore geometry and the pore size. Moreover, starting from such filled pores and decreasing the pressure (desorption), a hysteresis loop often appears and evaporation occurs at lower pressures than those observed for condensation. For very small pore sizes the condensation-evaporation steps are almost completely reversible, while in larger pores different types of hysteresis loops are observed, depending mainly on the shape and relative dimensions of the pores. In the hysteresis loop region the GCMC fails to adequately describe the gas-liquid coexistence. A direct calculation of the phase co-existence in this metastability region is achieved by using variations of the Gibbs ensemble (Panagiotopoulos, 1987; Mcgrother & Gubbins, 1999 ; Neimark & Vishnyakov, 2005).

(c) Nitrogen adsorption

N_2 adsorption isotherms at 77 K have been calculated for slit-shaped pores. Two types of adsorption behavior are observed similar to CO_2 case. For small micropores (0.8-1.2nm)

(figure 9a,b) a single layer is formed and pore filling occurs abruptly at low pressures (<10^{-4} bar), while further pressure increase does not change the amount adsorbed. As pore sizes increase the isotherm gradually changes to type IV. In small pressures, only a few molecules are occupying the sites near the pore walls. As the pressure increases, additional layers are adsorbed since finally the condensation pressure is reached and phase transition occurs. It must be also pointed out that pores smaller than 0.6nm are inaccessible to nitrogen molecules, due to the overlapping repulsive parts of the opposing wall potentials.

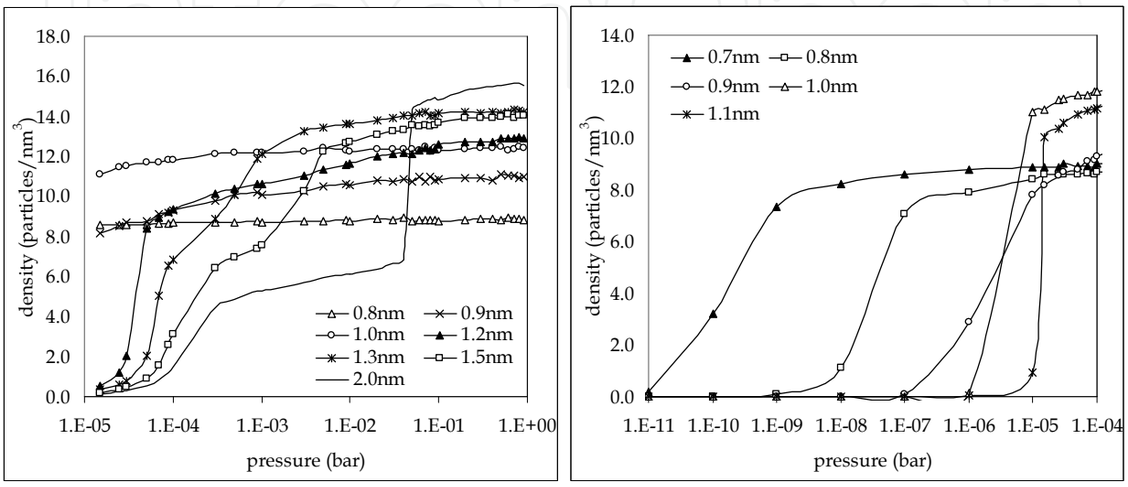

(a) (b)

Fig. 9. Nitrogen adsorption densities at 77K for selected slit-shaped pore widths a) up to the vapour pressure P_0=1 bar and b) for very low pressures.

N_2 adsorption isotherms at 77 K are commonly employed for pore size distributions determination of carbonaceous materials. Similar to the CO_2 behavior, nitrogen exhibits capillary condensation in much lower pressures than the vapor pressure, while the step in the isotherm occurs in different values of P/P_0 depending on the pore size. However, for pore widths between 0.7 and 1.0nm, the almost straight horizontal lines appearing for about the entire pressure range that is usually measured experimentally (10^{-5}-1 bar), imply that the method is not sensitive enough for small micropores, when based solely on N_2 data at 77 K.

3.3 GCMC simulation results – density profiles

GCMC simulations provide valuable information regarding the molecular packing and the adsorbed layers formed inside the individual pores at different pressures. The structure of the adsorbate in the pore is reflected by the local density profiles, namely the local number density at a distance *z* from the pore center (*z*=0 at the pore center). The corresponding local orientation of the molecules can also be obtained, as the ensemble average of the directional cosines of the fluid molecules in the cavity. Computationally such density and orientation profiles are obtained by dividing the pore into uniform segments and keeping record of the number of times a molecule is encountered inside each segment during the simulation.

In the case of H_2 the energetically favourable molecular configuration is rather simple, since the molecules are assumed to be chargeless and the fluid-fluid interactions do not have a prominent effect. Figure 10 presents the H_2 density profiles at 77 K in selected slit pores. The very fine pores are completely filled with one layer in their center. As the pore size

increases, the potential starts to reveal two minima and as a result two layers adjacent to the pore walls develop. No other dense layer is formed near the pore center, which is an evidence of the weak type of the fluid – fluid interactions.

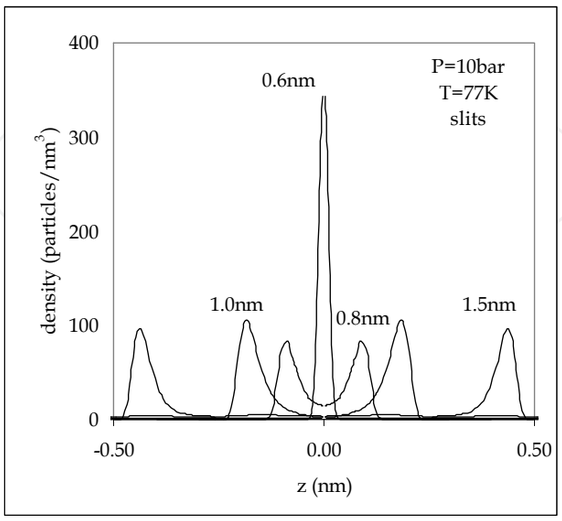

Fig. 10. Hydrogen local density profiles for different pore widths at 77K

Detailed CO_2 density profiles across the pore have been computed for the whole range of micropore widths (from 0.6 to 2.0 nm, in steps of 0.1 nm). The average fluid density in the micropores as a function of the pore width (H/2) is presented in Figure 11 for two pressures.

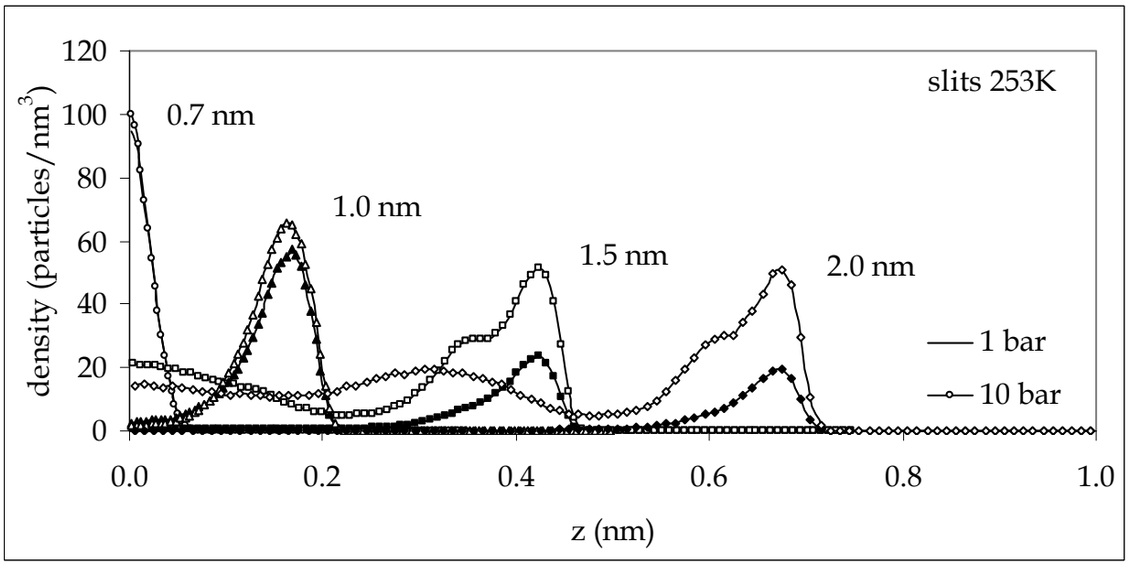

Fig. 11. CO_2 local density profiles for four pore sizes and two selected pressure levels at 253K (filled symbols 1 bar, open symbols 10 bar)

The density profiles reveal the formation of mono and multilayer adsorption films prior to capillary condensation. At low pressures the layer formation follows the same procedure as hydrogen, i.e. one dense layer in the center of the pore that is gradually transformed into

two lower density layers as the pore size increases. At higher pressures further densification of the layers in the smaller pores occurs, while new layers appear in wider pores. From the local orientation profiles it is concluded that the CO_2 molecules constituting the wall layers, tend to lie flat against the surface and this energetically favourable configuration (all three atoms of the molecule in the potential minimum) leads to high average densities in the pore, even at relatively low loadings. For higher pressures, a new distinct sublayer is developed over the primary layer. In the layer closer to the wall the molecules are lying parallel to it and in the second the molecules are oriented mostly normal to the pore wall. The presence of these two differently structured sublayers can be attributed to the quadrupole–quadrupole interactions, which have been reported to contribute essentially to the stability of such a T-like configuration of molecules. The role of the enhanced quadrupole–quadrupole interactions between the carbon dioxide molecules is crucial for sustaining these highly structured configurations. Once the quadrupole moment is eliminated from the simulations, the packing efficiency is lost. A detailed description concerning the local density and orientation profiles of CO_2 in carbon nanopores is given in previous works (Samios et al., 2000 ; Samios et al., 1997).

In Figure 12 the local density profiles of a slit shaped pore with width *H*=2.0 nm are compared for different temperatures (253 K, 273 K, 298 K and 308 K). It is evident that as temperature increases the wall layers become less dense and those near the pore center less pronounced. Moreover, the sublayer with molecule orientation normal to the wall i.e. the second layer, grows significantly and becomes more structured at lower temperatures. This result is consistent with the expected effect of temperature on the effect of the quadrupole–quadrupole interactions. For the cylindrical geometry the packing behavior of CO_2 is found rather similar. The layers are formed in the same distances from the walls, comparing pores of similar width (H~D). The main differences marked, concern the height and the width of the layers. In very narrow cylinders, the molecules cannot attain the most favorable orientation, as they are forced to align in a way almost parallel to the pore axis. Also, the sublayers in larger pores are more pronounced, even at high temperatures (298 K).

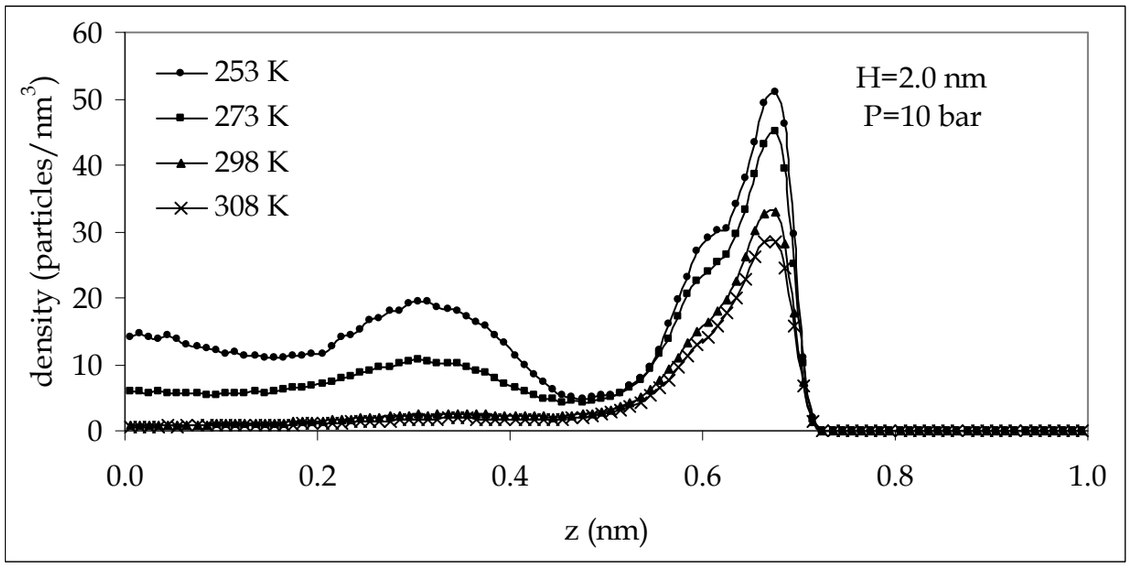

Fig. 12. Temperature effect on the CO_2 local density profiles for 2.0nm slit-shaped pore

3.4 Application of the simulated adsorption isotherms to the characterization of carbon porous materials – The pore size distribution (PSD) method

Gas sorption is considered as a well established method that can provide information on the pore size, the pore network connectivity, and other structural parameters of microporous and mesoporous materials (Kaneko, 1994; Yortsos, 1999). A large number of thermodynamic models of adsorption are commonly used to explain the features of the experimentally obtained isotherms of various gases and vapors. Some of them (Dubinin-Radushkevich, Dubinin-Astakhov and Dubinin-Stoeckli) use the Dubinin theory of pore filling to calculate the structural properties of the material (Greg & Sing, 1982), while others are modified t-curve methods implemented in micropores (MP and Horvarth – Kawazoe method) (Nicholson, 1994 ; Nicholson, 1996 ; Stoeckli et al., 2000). However, the results differ each time the calculation takes place, depending on the model used (Russell & LeVan, 1994 ; Kruk et al., 1998 ; Valladares et al., 1998).

The pore structure of a material is usually described in terms of the pore size distribution (PSD), namely the distribution of pore volume with respect to its size. Over the past 30 years several methods have been developed in this direction. The basic concept relies on the general dependence of the filling pressure and the pore width to the gas amount adsorbed. Since microscopic models can reproduce such a behavior adequately, the Density Functional Theory (Ravikovitch et al., 2006 ; Nguyen & Bhatia, 2004 ; Jagiello & Thommes, 2004) and the Monte Carlo simulation (Do & Do, 2005 ; Nguyen et al., 2005 ; Shao et al., 2004 ; Samios et al., 1997 ; Samios et al., 2000 ; Konstantakou et al., 2007a, Konstantakou et al., 2007b) are the most accepted methodologies. A review on both methods is given by (Do & Do, 2003). Regardless the theoretical approach, the probe molecule usually used for the determination of PSDs in porous carbons is nitrogen at 77 K. The experimental procedure is typical and relatively easy to perform. Additionally, the saturation vapor pressure of nitrogen allows for the accurate measurement of relative pressures over a wide range (commonly 10^{-5} – 0.995). Nitrogen is considered reasonably inert, inexpensive and in abundance, and also its sorption characteristics are well studied in literature. However, many microporous solids have pores with dimensions comparable to the size of nitrogen molecules, prohibiting the convenient diffusion, increasing the equilibration time and leading to significant under estimation of the adsorption isotherm (Rodriguez-Reinoso et al., 1988). Such diffusional limitations could influence adsorption especially in ultra-micropores (<0.7 nm).

Adsorption measurements at higher temperatures (near room temperature) and modest pressures (up to 20 bar) represent a more convenient alternative in terms of both experimental time and resolution (Garrido et al., 1987 ; Sweatman & Quirke, 2001) since the higher temperature facilitates molecules to access the narrower pores. For instance, a comparison between the PSDs calculated for the same material (activated carbon AX-21) using as probe molecules carbon dioxide at 293,1 K and nitrogen at 77 K, revealed that carbon dioxide can detect different pore sizes and in particular smaller than nitrogen (Scaife et al., 2000). Similarly, hydrogen is considered an excellent probe for very fine pores due to its small size, while at 77 K it is far above its supercritical temperature ensuring fast equilibration kinetics. Pertinent adsorption measurements have been used lately for the determination of PSDs (Jagiello & Thommes, 2004; Konstantakou et al., 2007a; Konstantakou et al., 2007b).

(a) Description of the method

The procedure for the determination of the optimal PSD of microporous carbonaceous materials requires two sets of data. The first set contains the experimental results of one or

more measured isotherms, depending on the number of gases used and / or the different temperatures applied. The other set (kernel) is composed of the corresponding (i.e. for the gases and temperatures used experimentally) simulated isotherms for different pore sizes. In order to derive the local isotherms (amount adsorbed for each pore size) the procedure described must be followed, i.e. accurate construction of pore models, precise representation of the probe molecule and appropriate selection of potential models. The method is based on the assumption that the experimental isotherm consists of a number of individual local (single pore) isotherms, each multiplied by a scaling factor (i.e. relative volume that each pore size occupies in the material). The adsorption integral has the following expression.

$$b(p) = \int_{H_{\min}}^{H_{\max}} A(H,p) \cdot x(H)\, dH \tag{12}$$

where H and p are the pore width and the pressure step respectively. $A(H,p)$ represents the adsorption kernel, $b(p)$ denotes the experimental isotherm and $x(H)$ is the unknown pore size distribution that covers a realistic range of pore sizes (H_{min}, H_{max}). Actually this is a linear system of m equations and n unknowns (i.e b=Ax) which can commonly be solved by minimizing the residual

$$\text{Minimize } \frac{1}{2}\|b - Ax\|^2 \text{ in respect to constraints} \tag{13}$$

The solution refers to a constrained least squares problem. The constraints are simple as we expect only non negative solutions and that the cumulative pore size distribution is equal to unity. Further constraints on the smoothness of x in order to force physically sound or appealing solutions, can also be imposed (see Konstantakou et al., 2007a; Konstantakou et al., 2007b and references therein). For this work the E04NCF routine from the NAG library (Gill et al., 1984; Stoer, 1971) has been implemented in order to perform the minimization.

(b) Application example

The technique is applied in the case of the KOH activated carbon AX-21, a microporous material with large surface area (made by Amoco Co. and kindly provided by S. R. Tennisson, MAST Carbon). In order to assure the reliability of the deduced PSD, several experimental isotherms were used, based on the argument that different adsorption isotherms in terms of temperatures and/or gases can probe different pore sizes. Therefore, instead of using N_2 at 77 K, high temperature CO_2 and H_2 isotherms at 77K have been considered. The measurements of the adsorption isotherms of CO_2 (253 and 298) and H_2 (77 K) were carried out in a pressure range 0–20 bar on the Intelligent Gravimetric Analyzer (IGA, Hiden Analytical Ltd.). Consequently, 25 GCMC adsorption isotherms were calculated overall, for each gas and temperature in the pore range H=0.6 - 3.0 nm (the pore range was divided in 25 equidistant intervals (pore groups) with 0.1 nm spacing between them). We must point out, that in the simulations the slit-shaped pore model was used, since it approximates better the sample structure.

In the first stage, three different PSDs were deduced (Fig. 13a), based on the individual CO_2 at 253 K, CO_2 at 298 K and H_2 at 77 K adsorption data and the respective experimental isotherms. As expected, all the distributions produced, are presenting dissimilar shape, as different probe molecules detect different pore groups.

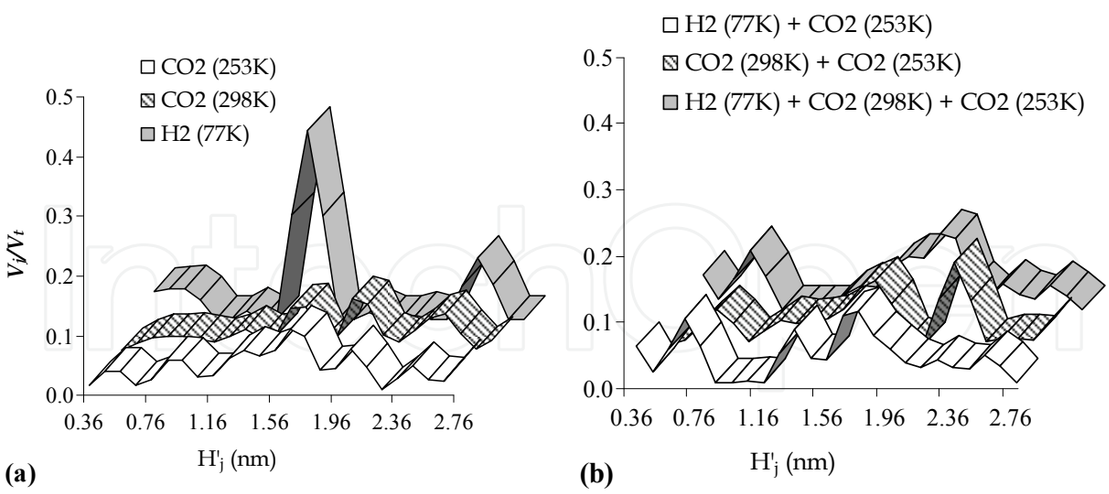

Fig. 13. PSDs based on a) individual adsorption isotherms, b) combinations of adsorption isotherms (V_j: volume of each class of pores and V_t: total pore volume).

The PSD obtained from the H_2 data is in marked contrast with that of CO_2, as it practically reveals 3 classes of pores centered at around H = 0.7, 1.6 and 2.7 nm. The simulated hydrogen isotherms loose gradually their curvature for pores sizes over 1.2 nm, turning to straight lines. In this respect, H_2 sorption isotherms cannot be used for the pore size characterization of samples having pores beyond the ultramicropore region, unless of course adsorption experimental data at much larger pressures are available. On the other hand, the PSDs of CO_2 at both temperatures display a much broader distribution of sizes spread over the entire range studied. Considering that the experimental isotherms were carried out at exactly the same equilibration pressures (up to 20 bar), much lower relative pressures have been measured at 298 K, while the measurement at 253 K contains the full relative pressure range (up to P/P_0 0.94). Consequently, the 298 K isotherm is expected to depict better the contribution of fine pores and the information given for the large pores is minimal. More complete information regarding the large pore region results from the 253 K isotherm.

By simultaneously inverting different adsorption integral equations, after including different combinations of experimental and GCMC data sets (but the same f(H) function), new PSDs are obtained (Fig.13b). The three "combined" PSDs are similar to each other, covering a long range of pore widths. The reliability of the PSDs is examined by using them in a reverse manner, i.e. for the prediction of the adsorption isotherms. The above approach has been followed for all the calculated PSDs and selected results are presented in Fig. 14. Of course all the PSDs can quite accurately predict their experimental counterparts, nevertheless experimental data on different molecules and/or temperatures cannot be accurately reproduced as presented in figure 14a (example of experimental CO_2 data at 253 K and predictions based on the PSDs of figure 13a). In contrast to the individual, the "combined" PSDs can better reproduce more than one experimental isotherm. As expected, the actual porous system of AX-21 is more accurately depicted by the PSD obtained from the combination of all the data. It should also be mentioned that the combination of the two "low relative pressure" isotherms (H_2 and CO_2 at 298 K) could not reproduce the CO_2 isotherm at 253 K (again because large pore information is missing). A straightforward result concerning the implementation of the technique is that the use of different probes is

essential for the valid characterization of polydisperse porous materials. The reliable PSD should contain complete information of a full relative pressure range isotherm and an accurate description of ultramicropores.

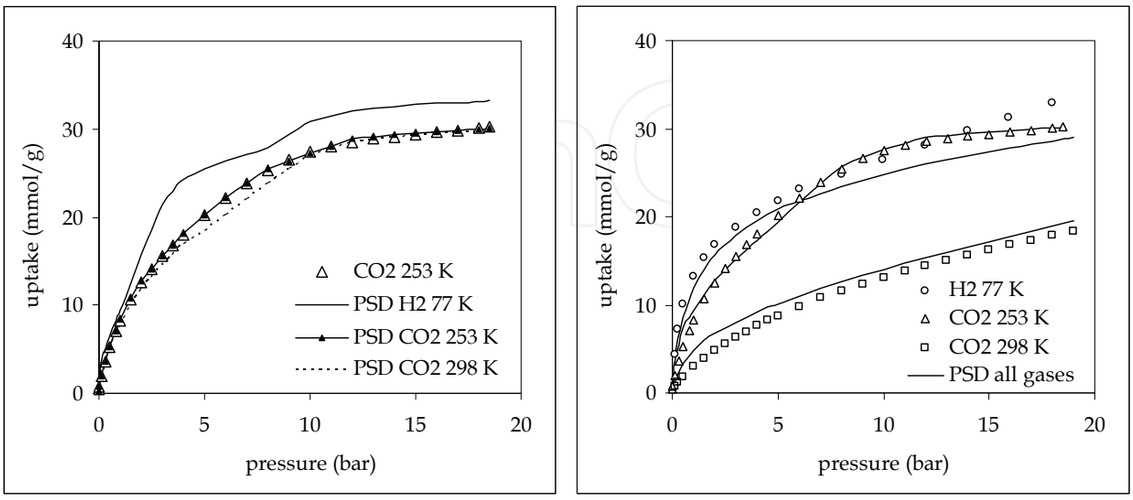

Fig. 14. a) Experimental CO_2 isotherm at 253 K (open triangles) and pertinent predictions based on the individual PSDs of figure 13a. b) Experimental isotherms (open circles: H_2 77 K, open triangles: CO_2 253 K, open squares: CO_2 298 K) on AX-21 and their predictions (lines) based on the combined PSDs using all data

4. Conclusions

The Grand Canonical Monte Carlo method is applied for the study of gas sorption (hydrogen, carbon dioxide and nitrogen) into narrow carbon pores of slit, cylindrical and conical shape. Depending on the gas, the calculations are performed for different temperatures (H_2 at 77 and 298K, CO_2 at 195.5, 253, 273, 298 and 308K and N_2 at 77K). Based on these results an analysis of the distinctive behaviour of each gas molecule when confined in carbon micropores is presented, while the effects of temperature and pore size/geometry is pointed out. In micropores the attractive forces between gas molecules and the surrounding pore walls are intense due to the overlapping solid wall potentials, resulting in single deep potential wells and thus enhanced gas adsorption. In the case of hydrogen, specific attention is given to the significance of employing the proper potentials for the description or the solid-fluid and fluid-fluid interactions. Evidently, quantum effects play an important role in hydrogen adsorption, especially at low temperatures and in the smallest pores.

Additionally, many interesting features are remarked from the calculated adsorption isotherms. Hydrogen sorption is in favour of very fine pores and low temperatures, while for wider pores adsorption capacity depends on the available surface area. In cones the enhanced adsorption is mainly attributed to the tip area, but also to the unique combination of local curvature and confinement. On the other hand, the polar nature of carbon dioxide and nitrogen molecules along with the introduction of wall forces, lead to interesting phase transitions. The simulation results also provide useful insight concerning the packing of the

gas molecules in the individual pores (local density and orientation profiles) as temperature and pressure change.

Finally, the simulated isotherms are used in combination with experimental data, in order to characterize microporous carbons and obtain optimal pore size distributions (PSDs). The adsorption isotherms have been used either individually or in a combined manner in order to deduce the PSDs and their reliability was examined by the ability to predict the experimental adsorption isotherms. Each probe molecule can detect different range of pore sizes. Thus, the combined approach was found to be capable of reproducing more accurately all the available experimental isotherms.

5. References

Alder, B.J. & Wainwright, T.E. (1960). Studies in Molecular Dynamics. II. Behavior of a Small Number of Elastic Spheres. J. Chem. Phys., 33, 6, (November 1960) 1439-51, 0021-9606

Allen, M.P. & Tildesley, D.J. (1987). Computer Simulation of Liquids, Clarendon press, 0198556454, Oxford

Aukett, P.N.; Quirke, N.; Riddiford, S. & Tennison, S.R. (1992). Methane adsorption on microporous carbons—A comparison of experiment, theory, and simulation. Carbon, 30, 6, 913-24, 0008-6223

Cracknell, R.F. (2001). Molecular simulation of hydrogen adsorption in graphitic nanofibres. Phys. Chem. Chem. Phys., 3, 11, 2091-7, 1463-9076

Darkrim, F. & Levesque, D.J. (1998). Monte Carlo simulations of hydrogen adsorption in single-walled carbon nanotubes. Chem. Phys., 109, 12, 4981-4, 0301-0104

Do, D.D. & Do, H.D. (2003). Pore Characterization of Carbonaceous Materials by DFT and GCMC Simulations: A Review. Adsorption Science and Technology, 21, 5, (June 2003) 389-423, 0263-6174

Do, D.D. & Do, H.D. (2005). Comparative adsorption of spherical argon and flexible n-butane in carbon slit pores—a GCMC computer simulation study. Colloids Surf. A: Physicochem. Eng. Aspects, 252, 1, (January 2005) 7-20, 0927-7757

Dresselhauss, M.S.; Dresselhauss, G. & Eklund, P.C. (1996). Science of fullerenes and carbon nanotubes, Academic Press, 0122218205, San Diego

Evans, R. & Tarazona, P. (1984). Theory of Condensation in Narrow Capillaries. Physical Review Letters, 52, 7, 557-60, 0031-9007

Everett D.H. (1972). Manual of Symbols and Terminology for Physicochemical Quantities and Units, Appendix II: Definitions, Terminology and Symbols in Colloid and Surface Chemistry. Pure Appl. Chem., 31, 4, 577-638, 0033-4545

Frenkel, D. & Smit, B. (1996). Understanding Molecular Simulation, from Algorithms to Applications, Academic Press, 0122673700, USA

Garrido, J.; Linares-Solano, A.; Martin-Martinez, J.M.; Molina-Sabio, M.; Rodriguez-Reinoso, F. & Torregosa, R. (1987). Use of nitrogen vs. carbon dioxide in the characterization of activated carbons. Langmuir, 3, 1, (January 1987) 76-81, 0743-7463

Ge, M. & Sattler, K. (1994). Observation of fullerene cones. Chem. Phys. Lett., 220, 3-5, 192-6, 0009-2614

Gill, P.E.; Murray, W.; Saunders, M.A. & Wright, M.H. (1984). Procedures for Optimization Problems with a Mixture of Bounds and General Linear Constraints. ACM Trans. Math. Software, 10, 3, (September 1984) 282-98, 0098-3500

Gotzias, A.; Heiberg-Andersen, H.; Kainourgiakis, M. & Steriotis, Th.A. (2010). Grand canonical Monte Carlo simulations of hydrogen adsorption in carbon cones. Applied Surface Science, 256, 17, 5226–31, 0169-4332

Gregg, S.J. & Sing, K.S.W. (1982). Adsorption Surface Area and Porosity, Academic Press, 0123009561, London

Gregg, S.J. & Sing, K.S.W. (1982). Adsorption, Surface Area and Porosity, Academic Press, 0123009561, London

Hansen, J.P. & McDonald, I.R. (1990). Theory of Simple Liquids; Academic Press, 0123705355, London

Harris, J.G. & Yung, K.H. (1995). Carbon Dioxide's Liquid-Vapor Coexistence Curve And Critical Properties as Predicted by a Simple Molecular Model. J. Phys. Chem., 99, 31, 12021-4, 0022-3654

Heiberg-Andersen, H. & Skjeltorp, A.T. (2007). Spectra of Conic Carbon Radicals. J. Math. Chem., 42, 4, (November 2007) 707-27, 0259-9791

Heiberg-Andersen, H.; Skjeltorp, A.T. & Sattler, K.J. (2008). Carbon nanocones: A variety of non-crystalline graphite. Non-Cryst. Solids 354, 47-51, (December 2008) 5247-9, 0022-3093

Iijima, S. (1991). Helical microtubules of graphitic carbon. Nature, 354, 6348, (November 1991) 56-7, 0028-0836

Jagiello, J. & Thommes, M. (2004). Comparison of DFT characterization methods based on N_2, Ar, CO_2, and H_2 adsorption applied to carbons with various pore size distributions. Carbon, 42, 7, (February 2004) 1227-32, 0008-6223

Kaneko, K. J. (1994). Determination of pore size and pore size distribution: 1. Adsorbents and catalysts. Membrane Sci., 96, 1-2, (November 1994) 59-89, 0376-7388

Konstantakou, M.; Samios, S.; Steriotis, Th.A.; Kainourgiakis, M.; Papadopoulos, G.K.; Kikkinides, E.S. & Stubos, A.K. (2007). Determination of Pore Size Distribution in Microporous Carbons Based on CO_2 and H_2 Sorption Data. Studies in Surface Science and Catalysis, 160, 543-50, 0167-2991

Konstantakou, M.; Steriotis, Th.A.; Papadopoulos, G.K.; Kainourgiakis, M.; Kikkinides, E.S. & Stubos, A.K. (2007). Characterization of Nanoporous Carbons by Combining CO_2 and H_2 Sorption Data with the Monte Carlo Simulations. Applied Surface Science, 253, 13, 5715-20, 0169-4332

Konstantakou, M.; Steriotis, Th.A.; Kikkinides, E.S. & Stubos, A.K. (2010). Monte Carlo simulations of CO_2 sorption in nanoporous carbons. Special Topics & Reviews in Porous Media – An International Journal, 1, 3, 205-13, 2151-4798

Krishnan, A.; Dujardin, E.; Treacy, M. M. J.; Hugdahl, J.; Lynum, S.; & Ebbesen, T, W (1997). Graphitic Cones and the nucleation of curved carbon surfaces, Nature, 388, (July 1997), 451-454 , 0028-0836

Kruk, M.; Jaroniec, M.& Choma, J. (1998). Comparative analysis of simple and advanced sorption methods for assessment of microporosity in activated carbons. Carbon, 36, 10, (October 1998) 1447-58, 0008-6223

Kuchta, B. & Etters, R.D.(1987). Calculated properties of monolayer and multilayer N_2 on graphite. Phys. Rev. B, 36, 6, 3400-06, 0163-1829

Lastoskie, C.; Gubbins, K.E. & Quirke, N. (1993). Pore size distribution analysis of microporous carbons: a density functional theory approach. J. Phys. Chem., 97, 18, 4786-96, 0022-3654

Liu, C.; Fan, Y.Y.; Liu, M.; Cong, H.T.; Cheng, H.M. & Dresselhaus, M.S. (1999). Hydrogen Storage in Single-Walled Carbon Nanotubes at Room Temperature. Science, 286, 5442, 1127-9, 0036-8075

Lowell, S. & Shields, J.E. (1991). Powder Surface Area and Porosity, Chapman Hall, 0412396904, London

Mcgrother, S.C. & Gubbins, K.E. (1999). Constant Pressure Gibbs Ensemble Monte Carlo Simulations of Adsorption into Narrow Pores. Molecular Physics, 97, 8, 955-65, 0026-8976

Metropolis, N.; Rosenbluth, A.W.; Rosenbluth, M.N.; Teller, A.H. & Teller, E. (1953). Equation of State Calculations by Fast Computing Machines. J. Chem. Phys., 21, 6, (June 1953) 1087-92, 0021-9606

Murthy, C.S.; O'Shea, S.F. & McDonald, I.R. (1983). Electrostatic interactions in molecular crystals Lattice dynamics of solid nitrogen and carbon dioxide. Molecular Physics, 50, 3, 531-541, 0026-8976

Neimark, A.V.; Ravikovitch, P.I. & Vishnyakov, A. (2003). Bridging Scales from Molecular Simulations to Classical Thermodynamics: Density Functional Theory of Capillary Condensation in Nanopores. J. Phys.: Condens. Matter, 15, 3, 347-65, 0953-8984

Neimark, A.V. & Vishnyakov, A. (2005). A Simulation Method for the Calculation of Chemical Potentials in Small, Inhomogeneous, and Dense Systems. The Journal of Chemical Physics, 122, 23, (June 2005) 234108-19, 0021-9606

Nguyen, T.X. & Bhatia, S.K. (2004). Probing the Pore Wall Structure of Nanoporous Carbons Using Adsorption. Langmuir, 20, 9, (March 2004) 3532-5, 0743-7463

Nguyen, T.X.; Bhatia, S.K. & Nicholson, D. (2005). Prediction of High-Pressure Adsorption Equilibrium of Supercritical Gases Using Density Functional Theory. Langmuir, 21, 7, (February 2005) 3187-97, 0743-7463

Nicholson, D. & Parsonage, N.G. (1982). Computer Simulation and the Statistical Mechanics of Adsorption, Academic Press, 0125180608, London

Nicholson, D.J. (1994). Simulation study of nitrogen adsorption in parallel-sided micropores with corrugated potential functions. Chem. Soc., Faraday Trans., 90, 1, 181-6, 0956-5000

Nicholson, D.J. (1996). Using computer simulation to study the properties of molecules in micropores. Chem. Soc., Faraday Trans., 92, 1, 1-10, 0956-5000

Nilson, R.H. & Griffiths, S.K. (1999). Condensation Pressures in Small Pores: An Analytical Model Based on Density Functional Theory. Journal of Chemical Physics, 111, 9, (June 1999) 4281-90, 1089-7690

Nilson, T.; Nicholson, D. & Kaneko, K. (2003). Temperature Dependence of Micropore Filling of N_2 in Slit-Shaped Carbon Micropores: Experiment and Grand Canonical Monte Carlo Simulation. Langmuir, 19, 14, 5700-5707, 0743-7463

Panagiotopoulos, A.Z. (1987). Adsorption and Capillary Condensation of Fluids in Cylindrical Pores by Monte Carlo Simulation in the Gibbs Ensemble. Molecular Physics, 62, 3, 701-19, 0026-8976

Ravikovitch, P.I.; Ó'Domhnaill, S.C.; Neimark, A.V.; Schuth, F. & Unger, K.K. (1995). Capillary Hysteresis in Nanopores: Theoretical and Experimental Studies of Nitrogen Adsorption on MCM-41. Langmuir, 11, 12, 4765-72, 0743-7463

Ravikovitch, P.I.; Vishnyakov, A. & Neimark, A.V. (2001). Density Functional Theories and Molecular Simulations of Adsorption and Phase Transitions in Nanopores. Physical Review E, 64, 1, 011602-22, 1539-3755

Ravikovitch, P.I.; Vishnyakov, A.; Neimark, A.V.; Ribeiro Carrott, M.M.L.; Russo, P.A. & Carrott, P.J. (2006). Characterization of Micro-Mesoporous Materials from Nitrogen and Toluene Adsorption: Experiment and Modeling. Langmuir, 22, 2, (November 2005) 513-6, 0743-7463

Rodriguez-Reinoso, F. & Linares-Solano, A. (1988). Microporous Structure of Activated Carbons as Revealed by Adsorption Methods, In: Chemistry and Physics of Carbon, vol. 21, P.A. Thrower (Ed.), Marcel Dekker, 978-0-8247-7939-9, New York

Russell, B.P. & LeVan, M.D. (1994). Pore size distribution of BPL activated carbon determined by different methods. Carbon, 32, 5, (January 1994) 845-55, 0008-6223

Ruthven, D.M. (1984). Principles of Adsorption and Adsorption Processes, Wiley – Interscience, 0471866067, New York

Samios, S.; Stubos, A.K.; Kanellopoulos, N.K.; Cracknell, R.F.; Papadopoulos, G.K. & Nicholson, D. (1997). Determination of Micropore Size Distribution from Grand Canonical Monte Carlo Simulations and Experimental CO_2 Isotherm Data. Langmuir, 13, 10 2795-2802, 0743-7463

Samios, S.; Stubos, A.; Papadopoulos, G.K.; Kanellopoulos, N.K. & Rigas, F. (2000). The Structure of Adsorbed CO_2 in Slitlike Micropores at Low and High Temperature and the Resulting Micropore Size Distribution Based on GCMC Simulations. J. Colloid Interface Sci., 224, 2, 272-90, 0021-9797

Scaife, S.; Kluson, P. & Quirke, N. (2000). Characterization of Porous Materials by Gas Adsorption: Do Different Molecular Probes Give Different Pore Structures?. J. Phys. Chem. B, 104, 2, (December 1999) 313-8, 1089-5647

Seaton, N.A.; Walton, J.P.R.B. & Quirke, N. (1989). A new analysis method for the determination of the pore size distribution of porous carbons from nitrogen adsorption measurements. Carbon, 27, 6, 853-61, 0008-6223

Sese, L.M. (1995). Feynman-Hibbs potentials and path integrals for quantum Lennard-Jones systems: Theory and Monte Carlo simulations. Mol. Phys., 85, 5, 931-47, 0026-8976

Shao, X.; Wang, W.; Xue, R. & Shen, Z. (2004). Adsorption of Methane and Hydrogen on Mesocarbon Microbeads by Experiment and Molecular Simulation. J. Phys. Chem. B, 108, 9, (February 2004) 2970-8, 1089-5647

Sosin, K.A. & Quinn, D.F. (1995). Using the high pressure methane isotherm for determination of pore size distribution of carbon adsorbents. J. Porous Mater., 1, 1, 111-19, 1380-2224

Steele, W.A. (1974). The Interaction of Gases with Solid Surfaces, Pergamon, 0080177247, Oxford

Stoeckli, F.; Guillot, A.; Hugi-Cleary, D. & Slasli, A.M. (2000). Pore size distributions of active carbons assessed by different techniques. Carbon, 38, 6, (February 2000) 938-41, 0008-6223

Stoer, J. (1971). On the Numerical Solution of Constrained Least-Squares Problems. SIAM J. Numer. Anal., 8, 2, (June 1971) 382-411, 0036-1429 (print) 1095-7170 (online)

Sweatman, M.B. & Quirke, N.J. (2001). Characterization of Porous Materials by Gas Adsorption at Ambient Temperatures and High Pressure. J. Phys. Chem. B, 105, 7, (January 2001) 1403-1411, 1089-5647

Tanaka, H.; Fan, J.; Kanoh, H.; Yudasaka, M.; Iijima, S. & Kaneko, K. (2005). Quantum nature of adsorbed hydrogen on single-wall carbon nanohorns. Mol. Simul., 31, 6-7, 465-74, 0892-7022

Tanaka, H.; Kanoh, H.; Yudasaka, M.; Iijima, S. & Kaneko, K. (2005). Quantum Effects on Hydrogen Isotope Adsorption on Single-Wall Carbon Nanohorns. J. Am. Chem. Soc., 127, 20, 7511-16, 0002-7863

Valladares, D. L.; Rodriguez-Reinoso, F. & Zgrablich, G. (1998). Characterization of active carbons: the influence of the method in the determination of the pore size distribution. Carbon, 36, 10, (October 1998) 1491-9, 0008-6223

Wang, Q. & Johnson, J.K. (1999). Computer Simulations of Hydrogen Adsorption on Graphite Nanofibers. J. Phys. Chem. B, 103, 2, 277-81, 1089-5647

Yortsos, Y.C. (1999). Probing Pore Structures by Sorption Isotherms and Mercury Porosimetry, In: Methods of the Physics of Porous Media, Volume 35 (Experimental Methods in the Physical Sciences, Po-Zen Wong, (Ed.), 69-117, Academic Press, 0124759823, New York

Applications of Monte Carlo Method in Science and Engineering
Edited by Prof. Shaul Mordechai

ISBN 978-953-307-691-1
Hard cover, 950 pages
Publisher InTech
Published online 28, February, 2011
Published in print edition February, 2011

In this book, Applications of Monte Carlo Method in Science and Engineering, we further expose the broad range of applications of Monte Carlo simulation in the fields of Quantum Physics, Statistical Physics, Reliability, Medical Physics, Polycrystalline Materials, Ising Model, Chemistry, Agriculture, Food Processing, X-ray Imaging, Electron Dynamics in Doped Semiconductors, Metallurgy, Remote Sensing and much more diverse topics. The book chapters included in this volume clearly reflect the current scientific importance of Monte Carlo techniques in various fields of research.

INTECH
open science | open minds

InTech Europe
University Campus STeP Ri
Slavka Krautzeka 83/A
51000 Rijeka, Croatia
Phone: +385 (51) 770 447
Fax: +385 (51) 686 166
www.intechopen.com

InTech China
Unit 405, Office Block, Hotel Equatorial Shanghai
No.65, Yan An Road (West), Shanghai, 200040, China
中国上海市延安西路65号上海国际贵都大饭店办公楼405单元
Phone: +86-21-62489820
Fax: +86-21-62489821

IntechOpen